# Partial loss-of-function alleles reveal a role for *GNOM* in auxin transport-related, post-embryonic development of *Arabidopsis*

**Niko Geldner[1,*], Sandra Richter[1], Anne Vieten[1], Sebastian Marquardt[1], Ramon A. Torres-Ruiz[2], Ulrike Mayer[1] and Gerd Jürgens[1,†]**

[1]ZMBP, Entwicklungsgenetik, Universität Tübingen, Auf der Morgenstelle 3, D-72076 Tübingen, Germany
[2]Lehrstuhl für Genetik, Technische Universität München, Wissenschaftszentrum Weihenstephan (WZW), Am Hochanger 8, D-85350 Freising, Germany

*Present address: Plant Biology Laboratory, The Salk Institute, 10010 North Torrey Pines Road, La Jolla, CA 92037, USA
†Author for correspondence (e-mail: gerd.juergens@zmbp.uni-tuebingen.de)

*Accepted 16 October 2003*

Development 131, 389-400
Published by The Company of Biologists 2004
doi:10.1242/dev.00926

## Summary

**The *Arabidopsis GNOM* gene encodes an ARF GDP/GTP exchange factor involved in embryonic axis formation and polar localisation of the auxin efflux regulator PIN1. To examine whether GNOM also plays a role in post-embryonic development and to clarify its involvement in auxin transport, we have characterised newly isolated weak *gnom* alleles as well as trans-heterozygotes of complementing strong alleles. These genotypes form a phenotypic series of *GNOM* activity in post-embryonic development, with auxin-related defects, especially in the maintenance of primary root meristem activity and in the initiation and organisation of lateral root primordia. Our results suggest a model for GNOM action mediating auxin transport in both embryogenesis and post-embryonic organ development.**

Key words: *GNOM*, Guanine-nucleotide exchange factor, Auxin transport, Lateral root formation, Canalisation hypothesis

## Introduction

The basic body pattern of higher plants as laid down during embryogenesis is apparent in the structure of the seedling and forms the basis for post-embryonic development. The *Arabidopsis* seedling can be sub-divided along the main, apical-basal, axis of polarity into primary shoot meristem, cotyledons, hypocotyl, root and primary root meristem. The two primary meristems are self-maintaining stem-cell systems that produce the majority of structures during post-embryonic development, such as vegetative leaves or flowers, as well as the tissue layers of the growing primary root. In addition, cell groups within the pericycle layer of the primary root give rise to lateral roots, thus forming a branched root system. Although much progress has been made over recent years in the analysis of patterning during embryogenesis and post-embryonic development, common molecular mechanisms remain to be elucidated (Jürgens, 2001).

One substance that has been implicated in a large number of growth and developmental processes is the plant growth regulator auxin. Auxin has been recognised to be polarly transported in an active, energy-dependent fashion (Rubery and Sheldrake, 1974). Since its initial description as the substance responsible for the differential growth of coleoptiles and phototropic bending some 70 years ago (Went, 1929), auxin has been implicated in many processes, ranging from gravitropic bending to lateral root formation and root regeneration, patterned outgrowth of leaf primordia, axillary bud growth and vascular tissue patterning (Taiz and Zeiger, 1998). Importantly, all these processes depend on the ability of auxin to be actively transported. A notable exception to this is perhaps its most basic function as a necessary factor for plant cells to continuously divide (Skoog and Miller, 1957). More recently, auxin has also been recognised as being important for embryonic patterning although its precise role remains to be clarified (Geldner et al., 2000).

Loss-of-function alleles of the *Arabidopsis GNOM* gene (also called *EMB30*) lead to severe defects in cell-to-cell alignment, as illustrated by a highly disordered vascular system, and in the establishment of the embryonic axis (Mayer et al., 1993). *gnom* seedlings invariably lack the most basal pattern element – the root meristem – and display variably fused cotyledons and a generally thickened and stunted axis. *GNOM* encodes a GDP/GTP exchange factor for small G-proteins of the ARF class that are important for coat recruitment and cargo-selective vesicle trafficking (Steinmann et al., 1999; Donaldson and Jackson, 2000). Thus, GNOM can be viewed as a regulator of intracellular vesicle trafficking. A role for GNOM in polar auxin transport was suggested by phenocopies of *gnom* seedlings that resulted from treatment of in vitro cultured embryos of *Brassica juncea* with auxin or auxin transport inhibitors (Liu et al., 1993; Hadfi et al., 1998). Later, the presumed link to auxin transport was supported by two additional lines of evidence. The putative auxin-efflux carrier PIN1 is mis-localised in *gnom* mutant embryos, and moreover, GNOM is involved in the continuous recycling of PIN1 from endosomes to the basal plasma membrane (Steinmann et al., 1999; Geldner et al., 2001; Geldner et al., 2003). However, it still cannot be completely ruled out that *gnom* mutants might be defective in some basic process of cell polarity establishment, which, as a secondary consequence, entails defects in auxin carrier localisation and polar auxin transport (Shevell et al., 2000).

A way to genetically distinguish between direct and indirect consequences of loss of gene activity is to analyse allelic mutants that range from total loss to subtle decrease in gene activity (Muller, 1932). For example, it has often been observed for genes involved in the early development of *Drosophila* that the primary function of the gene product can be inferred from a phenotypic series that correlates with residual gene activity (Nüsslein-Volhard et al., 1980; Roth et al., 1989). In the case of *gnom*, however, all available mutant alleles give essentially the same grossly abnormal seedling phenotype and thus do not provide information about the developmental process primarily affected. We have analysed weak phenotypes of *gnom* alleles that undergo post-embryonic development and display graded auxin-related defects. Our results suggest a primary function of GNOM in canalising auxin fluxes, which would explain its diverse developmental phenotypes.

## Materials and methods

### Plant material and growth conditions

Plants were grown at 24°C under long-day conditions. 5-7 day-old seedlings were used for all experiments and incubations. The alleles *gnom*$^{R5}$ and *gnom*$^{SIT4}$ were induced by mutagenesis of seeds with 0.3% EMS for 8 hours in the Landsberg *erecta* background. The complementing allele combination *gnom*$^{B4049}$*/emb30-1* in the Columbia background is a self-maintaining genotype since in each generation only the trans-heterozygous plants survive and are fertile. For growth on plates, seeds were surface sterilised as described previously (Berleth and Jürgens, 1993), plated on a basal medium containing 0.8% agar, 1% sucrose, 0.5× MS salts (pH 5.8) and plates were incubated upright under the conditions indicated above. Seeds were stratified at 4°C in the dark for 2-3 days. The shift to 24°C was defined as day zero of germination.

### Quantitative analysis of number of root meristematic cells

In order to get an estimate of the number of meristematic cells in the root tip, cells in the cortical cell file were counted from the cortex/endodermis initial up to the point where the cells were two to three times longer than wide. Subjective errors were only one to two cells since the transition to elongation is apparently very rapid.

### GUS staining procedures

Plants were treated with 90% acetone on ice for 30 minutes, then washed once for 10 minutes in GUS staining buffer and stained at 37°C in darkness in GUS staining buffer plus X-Gluc. GUS staining buffer (Malamy and Benfey, 1997): 100 mM sodium phosphate (pH 7), 0.1% Triton X-100, and 0.1-5 mM of each $K_3Fe^{III}(CN)_6$ and $K_4Fe^{II}(CN)_6$, depending on the line and signal strength. X-Gluc was added to a final concentration of 1 mg/ml from a 100× stock dissolved in dimethylformamide, which was freshly prepared.

### Establishment of GNOM-GUS transgenic lines

The *GNOM-GUS* reporter contruct was obtained by inserting PCR-amplified *GUS* open reading frame (ORF) into a 7.5 kb *GNOM* genomic fragment containing an *Avr*II restriction site at the 3′ end of the *GNOM* ORF, leading to a GNOM-GUS translational fusion that complemented the mutant phenotype. Cloning and transformation was done as described for *GNOM-myc* and *GNOM-GFP* constructs (Geldner et al., 2003). The PCR amplified region of the construct was sequenced. At least two independent lines were investigated for each aspect of GNOM expression.

### Sequence analysis of mutant alleles

Mutations in *gnom*$^{R5}$ and *gnom*$^{SIT4}$ were identified by amplifying the genomic region from homozygous mutant seedling DNA and subcloning it into pGEM. Two independently amplified and subcloned clones were sequenced and compared with Landsberg *erecta* sequence. Identified mutations were confirmed by restriction fragment polymorphism tests.

### Western blot

Western blots were done as described previously (Lauber et al., 1997). Proteins were separated on a 7.5% SDS-PAGE gel. Anti-GNOM serum (αGNS) (Steinmann et al., 1999) was diluted 1:4000.

### Histological analysis

Clearing of root tissues was done as described previously (Malamy and Benfey, 1997) or by mounting roots directly in a chloralhydrate solution and inspecting them immediately. Aerial tissues were prepared by shaking them for several hours in ethanol/acetic acid (3:1) at room temperature and then mounting them in chloralhydrate solution. Embryos were fixed on ice in ethanol/acetic acid (3:1) for 30 minutes and then cleared in chloralhydrate for inspection.

### Whole-mount immunofluorescence

PIN1 antibody was kindly provided by Klaus Palme (Gälweiler et al., 1998). Staining was done as described previously (Lauber et al., 1997), with the following modifications in order to increase signals in lateral root primordia. Roots were slightly squashed before dipping them into liquid nitrogen. Roots were treated with 3% Driselase solution at 37°C for 90 minutes starting with a 10 minute vacuum infiltration. They were then permeabilised in 20% DMSO, 3% Nonidet P-40. Primary and secondary antibody incubations were done at 37°C overnight, again after vacuum infiltration. All washes and incubations after the fixation step were done in phosphate-buffered saline (pH 7.4).

### Auxin and auxin transport inhibitor treatments

For induction of lateral root formation and for *DR5::GUS* staining of primary root tips, 10-20 seedlings grown on plates were transferred into 24-well culture plates containing 1 ml of liquid basal medium supplemented with auxin, or equal amounts of solvent for the control treatments, and incubated in a growth room for the indicated times. 100 mM stock solution in DMSO were used for naphthaleneacetic acid (NAA), dichlorophenoxyacetic acid (2,4-D) and N-1-naphthylphthalamic (NPA). For NPA-ring experiments seedlings were transferred onto new plates with their hypocotyl-root junction placed above a narrow strip of parafilm. A small agar block containing 500 μM NPA was placed on the parafilm, covering the hypocotyl-root junction of the seedlings.

### Statistical analysis of results

P values indicated for measurements of inflorescence and root lengths, lateral root densities and gravitropic responses were obtained using a two-sided Student's *t*-test assuming unequal variances. *P* values indicated for numbers of rosette side branches were obtained using a $\chi^2$-test after grouping classes 1-2 and classes 6-8. The *P* values for the number of collapsed roots were obtained with a two-by-two $\chi^2$-test (one degree of freedom). The *P* value for the distribution of bolting time was obtained by grouping measurements into two categories, one before and one after day 20 and applying Fisher's exact test, calculated at home.clara.net. All other calculations were done using Microsoft® Excel 2002. All error bars in graphs indicate standard errors of the mean.

## Results

### Post-embryonic expression of *GNOM*

GNOM expression has only been assessed by western blot analysis of protein extracts from various organs (Steinmann et al., 1999). To determine the developmental expression pattern

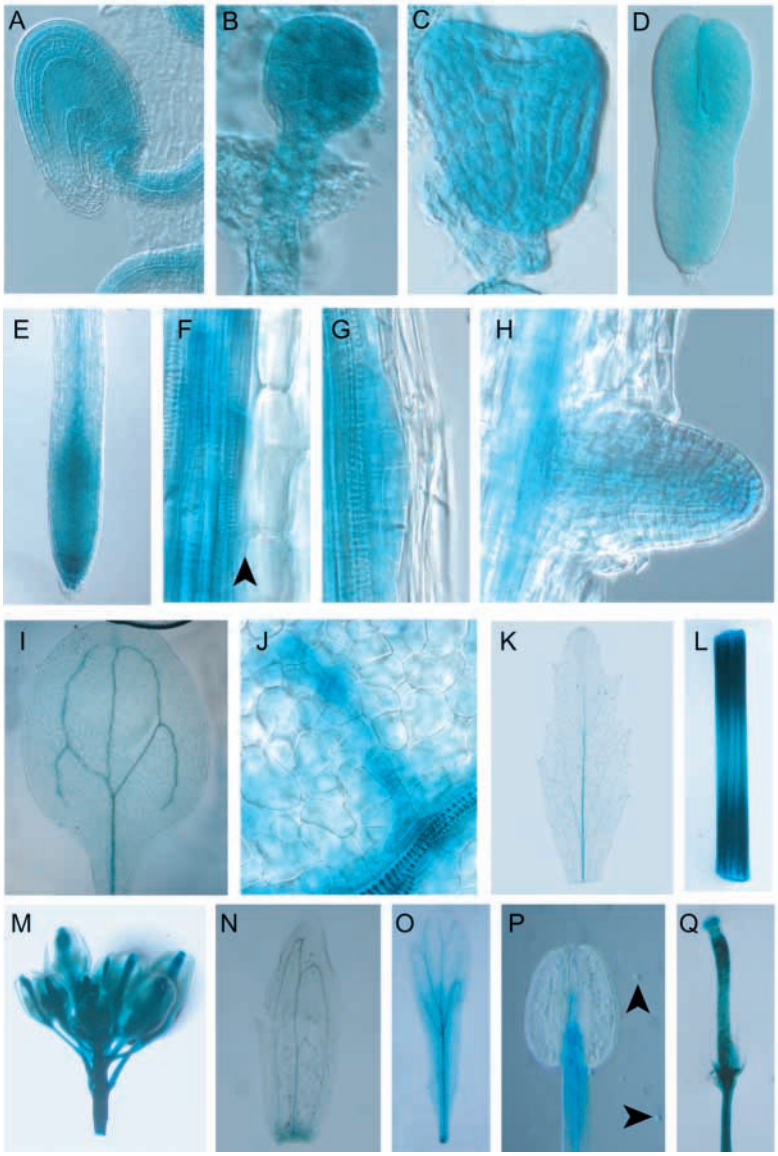


**Fig. 1.** GNOM is expressed during embryonic and post-embryonic development. GUS staining of transgenic *GNOM-GUS* plants. (A) Mature ovule. (B-D) Embryos at (B) dermatogen, (C) heart and (D) torpedo stages. (E-H) Seedling roots: (E) primary root tip; (F) vascular bundle; note strong difference in staining between vascular bundle and endodermis (arrowhead marks border); (G) young lateral root primordium; (H) emerged lateral root primordium. (I) Cotyledon. (J) Undifferentiated vascular strand. (K) Late rosette leaf. (L) Inflorescence stem segment. (M) Young flower buds. (N-Q) Floral organs: (N) sepal; (O) petal; (P) stamen, note weak GUS signal in mature pollen grains (arrowheads); (Q) gynoecium.

of *GNOM*, we inserted the *GUS* gene in-frame into a 7.5 kb genomic fragment of *GNOM*, which had been shown to complement the mutant phenotype (Geldner et al., 2003), and generated *GNOM-GUS* transgenic plants. Strong GUS activity was detected in the maternal sporophytic tissue of the ovule (Fig. 1A). During embryogenesis, GUS expression was more or less ubiquitous, possibly weaker in the suspensor (Fig. 1B,C) and slightly stronger in vascular primordia (Fig. 1D). In seedling roots, GUS staining was ubiquitous in the meristem, but restricted to cells of the vascular cylinder in the elongation and differentiation zones (Fig. 1E-F). GUS activity was also detected in developing lateral roots from early stages on, eventually resembling the expression pattern in the primary root (Fig. 1G,H and data not shown). In the cotyledons, GUS staining was very weak in mesophyll cells whereas the vascular strands and undifferentiated vascular tissues were clearly stained (Fig. 1I,J). Comparable staining patterns were detected in rosette and cauline leaves (Fig. 1K and data not shown). Inflorescence stems stained strongly, especially in the vascular bundles, the growing inflorescence apex and young floral buds (Fig. 1L,M). GUS expression in the flower varied between organs. It was almost undetectable in sepals (Fig. 1N) whereas the vasculature of petals was clearly stained (Fig. 1O). Stamens showed strong staining of the filament but no staining in the anther except for pollen grains (Fig. 1P). The entire gynoecium was strongly stained (Fig. 1Q). In summary, *GNOM* appears to be strongly expressed in actively dividing or elongating cells but only weakly or not at all in differentiated tissues other than the vasculature.

## Weak *gnom* phenotypes in post-embryonic development

More than 40 independently isolated *gnom* alleles display the characteristic strong embryo and seedling phenotype described previously (Mayer et al., 1993). Many of those alleles carry nonsense mutations before or in the central catalytic Sec7 domain, whereas the few identified missense mutations, such as $gnom^{B4049}$ and *emb30-1* map exclusively to the Sec7 domain (Busch et al., 1996) (Fig. 2A). No mutation was identified in the entire C-terminal half of the protein. However, two independently isolated recessive mutants with variably fused cotyledons (see below) turned out to be weak *gnom* alleles carrying mutations in this region. These mutants mapped close to the *GNOM* locus and were not complemented by *gnom* alleles, their phenotype being dominant over the strong *gnom* phenotype, which indicated that these lines have reduced *GNOM* function. Sequencing of these two EMS-induced alleles revealed mutations in the *GNOM* gene. $gnom^{SIT4}$ had a G to A exchange that would truncate the protein after amino acid 983, and $gnom^{R5}$ had a 1 bp deletion near the 3′-end of the open reading frame, resulting in an out-of-frame stop codon 51 bp downstream of the mutation (Fig. 2A). The sequencing results were confirmed by western blot. GNOM protein from $gnom^{R5}$ was slightly smaller and consistently less abundant than GNOM full-length protein (Fig. 2B). Thus, the reduction of *GNOM* function resulting from this allele could be due to decreased protein accumulation rather than loss of the C-terminal 86 amino acids. $gnom^{SIT4}$ plants also lacked GNOM full-length protein. The mutant protein was not reliably detected at the expected size of 110 kDa because of a cross-reacting band (Fig. 2B). This truncated protein, despite the

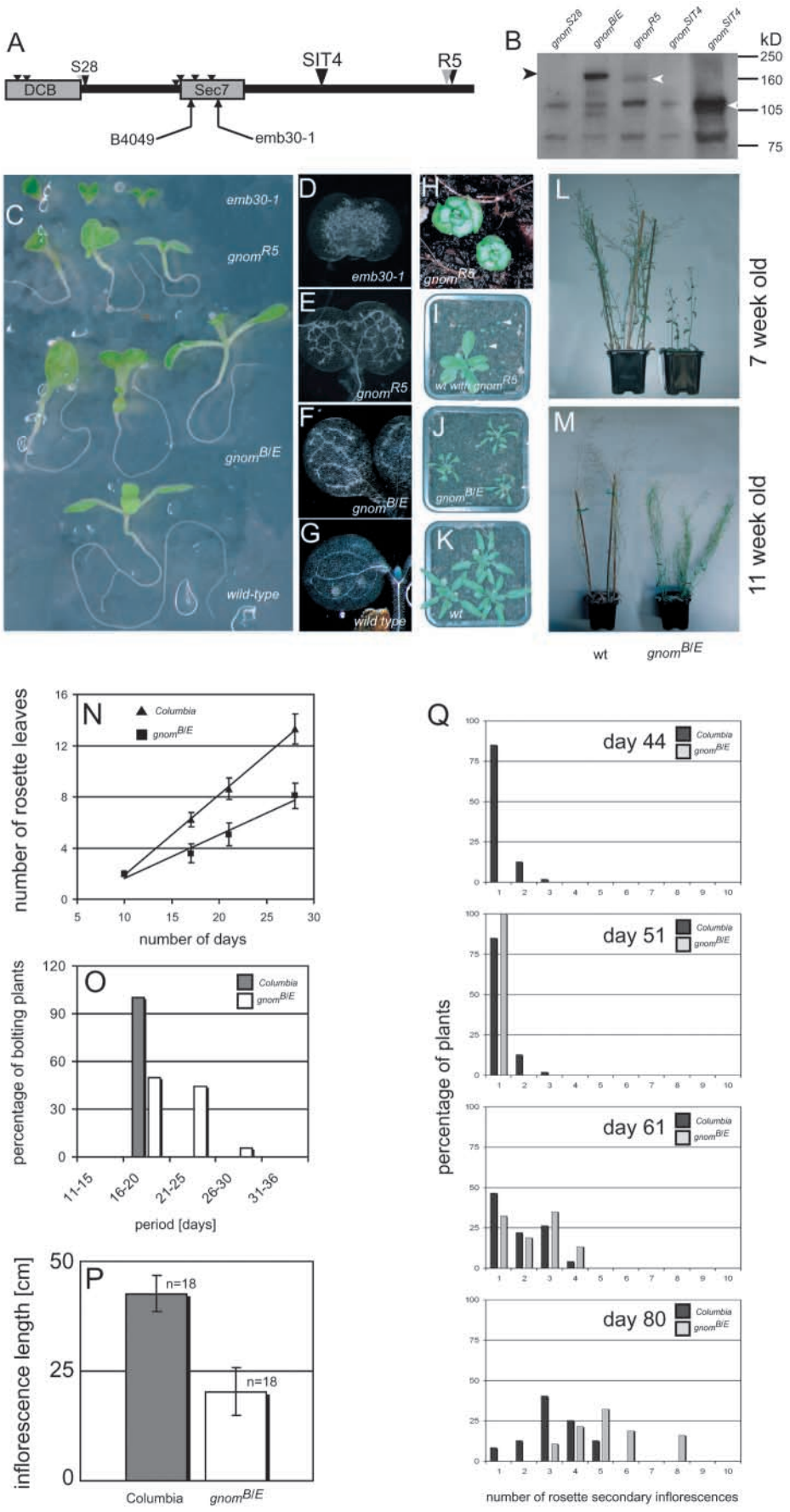


**Fig. 2.** Weak alleles of *gnom* have a number of post-embryonic growth phenotypes. (A) Diagram of GNOM protein depicting the N-terminal dimerisation and cyclophilin-binding (DCB) domain (Grebe et al., 2000) and the central, catalytic Sec7 domain (Shevell et al., 1994). Small arrowheads indicate positions of premature stop codons leading to strong *gnom* phenotypes, grey/black double-arrowhead indicates splice-site mutation in $gnom^{S28}$ (grey), leading to an out-of-frame stop (black). Arrows indicate positions of the two complementing missense mutations (Busch et al., 1996). Large arrowheads indicate mutations leading to premature stops in the weak alleles. $gnom^{SIT4}$ is a CAA to TAA nonsense mutation of codon 984. Grey/black double arrowhead indicates the AGC to AC frame-shift mutation of codon 1369 leading to an out-of-frame stop (black) in $gnom^{R5}$. (B) Immunoblot of strong and weak *gnom* alleles. $gnom^{B4049}$/*emb30-1* ($gnom^{B/E}$), full-length mutant protein (165 kDa, black arrowhead); $gnom^{S28}$, negative control. White arrowheads indicate the expected positions of the truncated proteins of $gnom^{R5}$ (155 kDa) and $gnom^{SIT4}$ (110 kDa). Four-times as much protein was loaded on the rightmost lane as on the lane to its left. (C) Overview of phenotypic series of 8-day-old seedlings from a strong (*emb30-1*), a weak ($gnom^{R5}$) and a very weak *gnom* line ($gnom^{B/E}$). (D-G) Cotyledon vasculature of (D) strong, (E) weak, (F) very weak *gnom*. (G) Vasculature of wild type. (H-K) Rosette stage plants: (H) $gnom^{R5}$; (I) size comparison between wild-type sister and $gnom^{R5}$; arrowheads indicate extremely dwarfed $gnom^{R5}$ plantlets; (J) $gnom^{B/E}$; (K) wild type. (L-M) Flowering shoots of (L) 7-week and (M) 11-week-old plants of *Col* and $gnom^{B/E}$. (N) Plastochrons of *Col* and $gnom^{B/E}$. $n$=31 and $n$=43 per time-point for *Col* and $gnom^{B/E}$, respectively. (O) Comparative histogram between Col and $gnom^{B/E}$, showing percentages of plants bolting per indicated time period. $n$=19 and $n$=18 for *Col* and $gnom^{B/E}$, respectively. There was a significant difference between the genotypes ($P$<0.001). (P) Primary inflorescence height of *Col* and $gnom^{B/E}$ at maturity. There was a significant difference between the genotypes ($P$<0.001). (Q) Histogram of percentage of plants with a given number of rosette side branches at several time points. $n$=47 and $n$=37 for *Col* and $gnom^{B/E}$, respectively. At day 80, there was a significant difference between the genotypes ($P$<0.001).

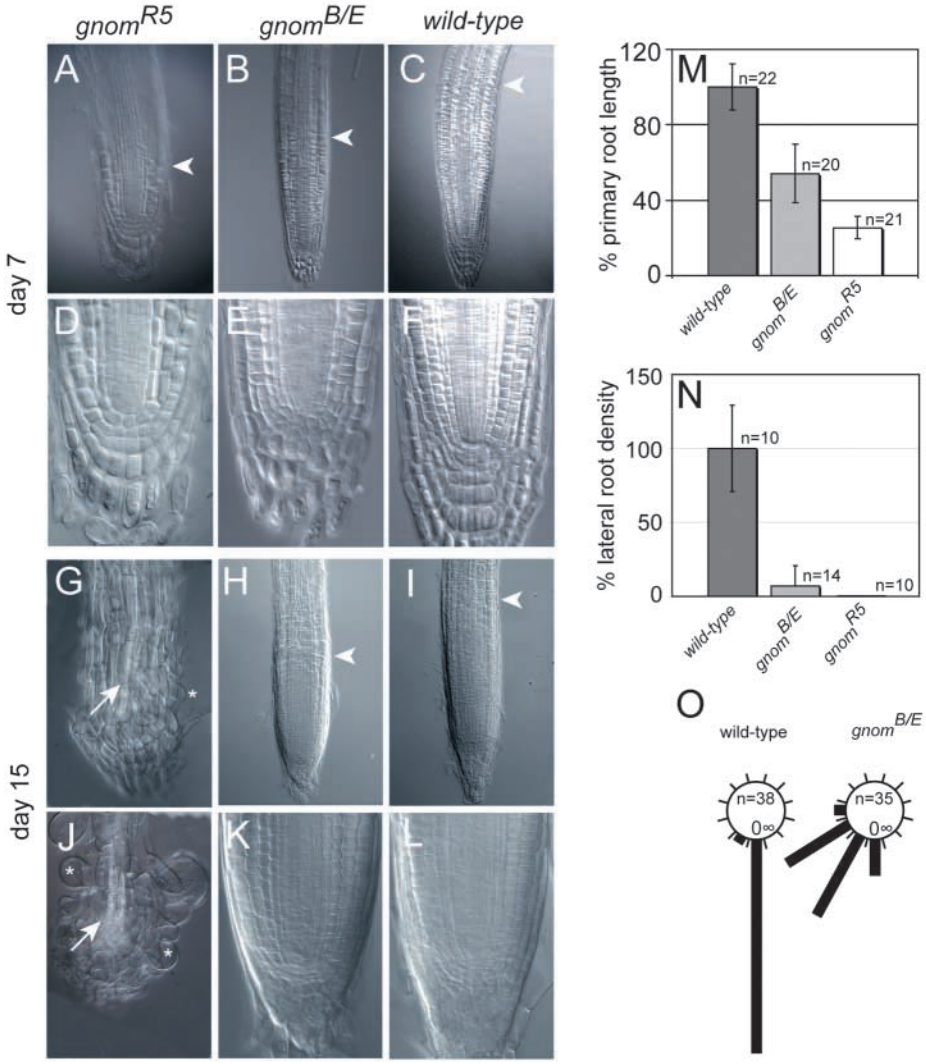


**Fig. 3.** Weak alleles are defective in meristem maintenance. (A-L) Primary root meristems of *gnom*$^{R5}$, *gnom*$^{B/E}$ and wild-type at (A-F) day 7 and (G-L) day 15. (A,D,G,J) *gnom*$^{R5}$, (B,E,H,K) *gnom*$^{B/E}$, (C,F,I,L) wild type. (D-F,K,L) Higher magnifications of A-C,H,I, respectively. Arrowheads in A-C,H,I indicate approximate position of the onset of cell elongation. (G,J) Two examples of collapsed *gnom*$^{R5}$ root meristems at day 15 (arrows, vascular strands; asterisks, bloated root hairs). (M) Root lengths of *gnom*$^{B/E}$ and *gnom*$^{R5}$ relative to wild type. Both genotypes are significantly different from wild-type control ($P$<0.001). (N) Lateral root density of *gnom*$^{B/E}$ and *gnom*$^{R5}$ relative to wild type. Note that in *gnom*$^{R5}$, lateral roots were never observed. Both genotypes are significantly different from wild-type control ($P$<0.001). (O) Gravitropic growth response of *gnom*$^{B/E}$ as compared to wild type. Seedlings grown upright were turned by 135° and re-alignment to the gravity vector was recorded after 36 hours. Each root was assigned one of twelve 30° sectors. Genotypes were significantly different ($P$<0.001).

deletion of nearly the entire C-terminal region, evidently retained residual GNOM function, as *gnom*$^{SIT4}$ was phenotypically similar to, or only slightly more affected than, *gnom*$^{R5}$. This clearly demonstrates that the large and uncharacterised part of the GNOM protein is not absolutely required for its function. In this work, we used *gnom*$^{R5}$ for all experiments.

Two missense *gnom* alleles, *gnom*$^{B4049}$ and *emb30-1* complemented each other, producing fertile plants (Busch et al., 1996). However, *gnom*$^{B4049}$/*emb30-1* trans-heterozygous plants (designated *gnom*$^{B/E}$ hereafter) displayed a number of post-embryonic defects that were less severe than those of *gnom*$^{R5}$, which will be described below. An allelic series of decreasing phenotypic strength – strong *gnom* alleles > *gnom*$^{R5}$ > *gnom*$^{B/E}$ > wild-type – was apparent from the seedling morphology (Fig. 2C). About one-third of the *gnom*$^{R5}$ seedlings displayed partial or complete fusion of cotyledons whereas the stronger collar-cotyledon phenotype was observed very rarely. Importantly, none of the *gnom*$^{R5}$ seedlings lacked a primary root, which is an invariable phenotype of strong *gnom* alleles. However, *gnom*$^{R5}$ seedlings with two separate cotyledons were nearly indistinguishable from wild-type 4-5 days after germination, except for their slightly darker cotyledons with very stunted petioles. After several days of growth, however, *gnom*$^{R5}$ seedlings differed from wild-type in their severely reduced expansion of hypocotyl and cotyledons and their shorter root. Compared to *gnom*$^{R5}$ seedlings, *gnom*$^{B/E}$ seedlings also displayed variable fusion of cotyledons at similar rates. However, their expansion growth was much less affected and their root was only slightly shorter than in wild-type (Fig. 2C). A clear series of phenotypic strength was also observed for the vascular tissue of cotyledons, with strong *gnom* alleles producing a high density of randomly oriented tracheid cells (Mayer et al., 1993) (Fig. 2D). *gnom*$^{R5}$ plants differentiated less vascular tissue than did those with strong *gnom* alleles, and some alignment of tracheid cells was recognisable (Fig. 2E). Finally, *gnom*$^{B/E}$ seedlings had rather well-aligned vascular strands, which often failed to be interconnected and were still wider than the narrow strands of wild-type cotyledons (Fig. 2F,G).

Unlike plants with strong alleles, *gnom*$^{R5}$ and *gnom*$^{B/E}$ plants were able to grow on soil. *gnom*$^{R5}$ seedlings developed into extremely dwarfed plants with very small and epinastic rosette leaves (Fig. 2H,I), which often died at the rosette stage, while rare escapers produced an inflorescence with a single, extremely tiny flower (data not shown). *gnom*$^{B/E}$ plants were only slightly dwarfed and had narrow, curled-down rosette leaves (Fig. 2J,K). *gnom*$^{B/E}$ plants produced inflorescences although flowering was delayed (Fig. 2L). At maturity, *gnom*$^{B/E}$ had produced more secondary inflorescences than

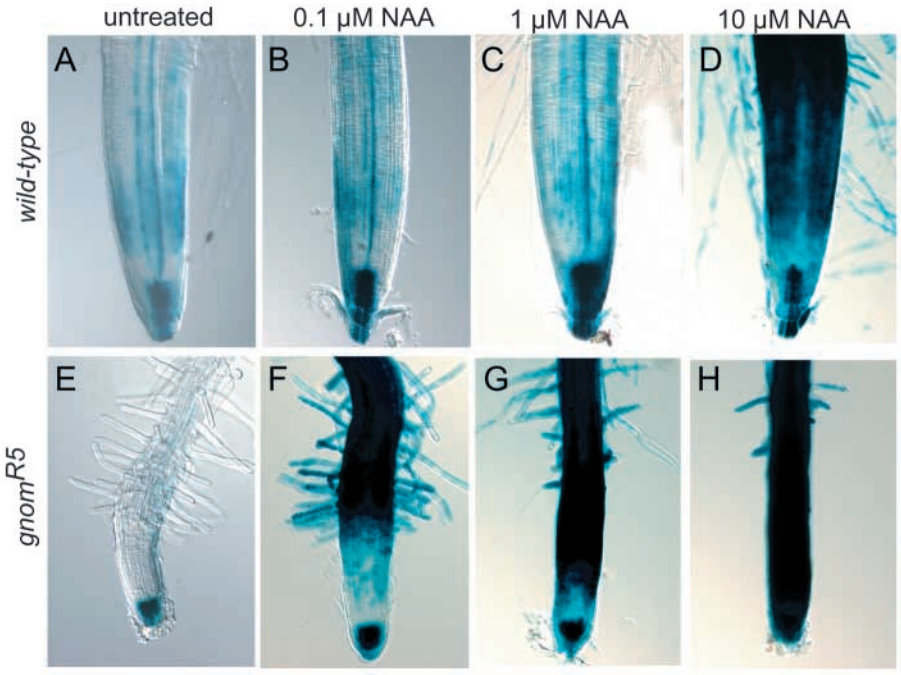


**Fig. 4.** Auxin response gradients in *gnom*$^{R5}$ root tips break down upon auxin treatment. *DR5::GUS* signals in (A-D) wild type, (E-H) *gnom*$^{R5}$. (A,E) Untreated, (B,F) 0.1 µM NAA, (C,G) 1 µM NAA, (D,H) 10 µM NAA. Treatment was done for 24 hours. Note that *DR5::GUS* response gradients are severely affected at 1 µM NAA in *gnom*$^{R5}$ (G), whereas in wild type a comparable change can only be observed at tenfold higher concentration (D).

wild type, which correlated with delayed onset of senescence (Fig. 2M). To better understand the phenotypic differences between *gnom*$^{B/E}$ and wild type, we performed quantitative growth measurements. *gnom*$^{B/E}$ formed rosette leaves at a significantly slower rate, which could acount for the delayed onset of flowering (Fig. 2N). In addition, the onset of flowering was much more variable in *gnom*$^{B/E}$ plants than in wild type (Fig. 2O). At maturity, the primary inflorescences were significantly shorter in *gnom*$^{B/E}$ than in wild type (Fig. 2P). When investigating the dynamics of secondary inflorescence formation from the axils of rosette leaves (Fig. 2Q), we observed an initial delay in *gnom*$^{B/E}$ plants. When wild-type plants started to senesce, however, *gnom*$^{B/E}$ plants continued to form new secondary inflorescences, eventually leading to more rosette side branches and an overall bushy appearance.

### Weak *gnom* alleles produce defects in root meristem maintenance, lateral root formation and gravitropism

Another striking aspect of the *gnom*$^{R5}$ phenotype was the slow rate of post-embryonic root elongation that became apparent after a few days of growth on plates. Compared to 7-day-old wild-type seedlings, *gnom*$^{R5}$ and *gnom*$^{B/E}$ displayed a significantly shortened division zone in the root (7.5±1.1 meristematic cells in *gnom*$^{R5}$ ($n$=8) as compared to 24.9±3.3 in wild type ($n$=8), $P$<0.001) (Fig. 3A-C). The overall meristem organisation was nonetheless roughly normal (Fig. 3D-F). Individual cell files originated from the centre of the meristem, no supernumerary tissue layers were observed, and a normally organised root cap was present. The quiescent centre and surrounding initials were sometimes well ordered (Fig. 3D) but sometimes fairly disorganised (Fig. 3E) in both *gnom*$^{R5}$ and *gnom*$^{B/E}$, as compared to wild type (Fig. 3F). After 15 days of growth, however, dramatic differences were observed between *gnom*$^{R5}$ and *gnom*$^{B/E}$. Many *gnom*$^{R5}$ roots were completely collapsed, with cell differentiation occurring at the very root tip, as evidenced by the presence of elongated cells, differentiated vascular strands and root hairs in that region (Fig. 3G,J). In contrast, *gnom*$^{B/E}$ and wild-type meristems (Fig. 3J,K) were intact, although the highly ordered cellular pattern of young roots was not present, either in the wild type or in *gnom*$^{B/E}$ (compare Fig. 3H,K with I,L). Thus, *GNOM* function is apparently not only needed for the establishment of an embryonic root meristem, but also for maintaining the activity of meristematic cells and preventing their differentiation. Although the collapse of the root meristem would explain why *gnom*$^{R5}$ roots eventually cease to grow, it cannot account for the short-root phenotype in 7-day-old seedlings, which might rather reflect fewer actively dividing cells in the meristem (Fig. 3M).

Both *gnom*$^{B/E}$ and *gnom*$^{R5}$ seedlings were also strongly affected in lateral root formation. Whereas *gnom*$^{B/E}$ still formed very few lateral roots, *gnom*$^{R5}$ did not form any (Fig. 3N). Microscopic inspection of whole-mount preparations indicated that this defect was not due to early arrest of primordium development but rather caused by a failure to initiate lateral root primordia. Defects in lateral root formation and in primary root elongation are both indicative of defects in auxin transport or perception (Casimiro et al., 2003). Another auxin-mediated process is the root gravitropic bending response, which we analysed in *gnom*$^{B/E}$ by recording the re-alignment of root tips after 36 hours of gravistimulation. In contrast to wild-type, *gnom*$^{B/E}$ was not able to correctly re-orientate its root growth to the vector of gravity (Fig. 3O). Taken together, this triple defect of the weak *gnom* lines in primary root elongation, lateral root formation and gravitropic growth strongly suggests that *GNOM* is important for auxin transport-mediated regulation of root development.

### *gnom*$^{R5}$ root tips have a reduced capacity to maintain auxin gradients in the presence of auxin

In order to assess more directly the auxin transport defects of *gnom* in we crossed the *DR5::GUS* reporter into *gnom*$^{R5}$. The *DR5::GUS* construct is highly responsive to auxin, being activated by auxin in all root cells (Ulmasov et al., 1997; Sabatini et al., 1999). Therefore, *DR5::GUS* is a useful marker to visualise auxin-response gradients in the root. In young *gnom*$^{R5}$ roots with an intact meristem, the GUS signal was nearly normal, except for two stripes of vascular cells that were observed in wild-type upon staining for 1-2 hours (Fig. 4A,E). As reported previously (Friml et al., 2002), treatment of wild

type with low concentrations of the transportable auxin NAA did not lead to strong alterations in *DR5::GUS* staining (Fig. 4B,C). Apparently, the auxin-transport system of the root tip has a high capacity to maintain response gradients in the presence of exogenous auxin, which is thought to be due to efficient canalisation of auxin to sites of degradation in the root tip (Friml et al., 2002). At 10 μM NAA, however, the *DR5::GUS* distribution changed dramatically. Strong GUS staining appeared in all tissue layers in the division zone of the root, leaving only a narrow strip of less stained cells immediately above the columella peak (Fig. 4D). *gnom$^{R5}$* root tips were dramatically more sensitive to exogenous auxin applications. Already at 0.1 μM NAA, strong GUS staining expanded from the differentiation zone into the division zone (Fig. 4F). At 1 μM NAA, the staining pattern very much resembled that of wild type at a tenfold higher concentration (Fig. 4G, compare with D). Ten μM NAA resulted in strong GUS staining of the entire root (Fig. 4H). Thus, the root meristem defects of weak *gnom* alleles correlated with a reduced capacity to transport auxin in the root.

### Auxin rescues and auxin transport inhibitors phenocopy *gnom$^{R5}$*

The collapse of the *gnom$^{R5}$* root meristem could well be explained by insufficient auxin supply, which eventually leads to differentiation of initials and root growth arrest. However, systemic treatment of roots with auxin transport inhibitors, such as NPA, increases, rather than decreases, auxin in the root meristem, resulting in more and disordered cell divisions, which is opposite to the *gnom$^{R5}$* phenotype (Ruegger et al., 1997; Sabatini et al., 1999). This systemic NPA effect was attributed to local inhibition of auxin transport to sites of degradation in the root tip (Friml et al., 2002). With this in mind, we attempted to preferentially inhibit auxin transport from aerial tissues rather than to block transport in the root tip itself. We therefore applied NPA locally to the hypocotyl-root junction of wild-type seedlings and recorded primary root growth and lateral root density after 15 days of growth. Lateral root density was dramatically decreased, as previously reported (Reed et al., 1998) (Fig. 5A). Primary root growth responded in two different ways. Either roots grew more slowly and growth was arrested after a few days or primary root elongation was apparently unaffected although the root became clearly agravitropic (data not shown). On average, however, primary root elongation was significantly diminished (Fig. 5B). In a representative experiment, 10 out of 29 roots grew less than 2 cm in 15 days. These growth-arrested roots had a severely shortened or completely collapsed root meristematic zone, with cell elongation, vascular differentiation and root hair outgrowth occurring at the extreme root tip (Fig. 5D). By these criteria NPA-treated wild-type roots resembled those of *gnom$^{R5}$* plants (Fig. 5C-E). In addition, all plantlets were dwarfed, had dark green epinastic leaves and were nearly indistinguishable from *gnom$^{R5}$* plantlets (Fig. 5F-H). Thus, local NPA application to the hypocotyl-root junction phenocopied essential features of the *gnom$^{R5}$* phenotype. To further examine whether the *gnom$^{R5}$* root meristem phenotype was caused by reduced auxin levels, we attempted to rescue primary root growth by exogenous application of auxin. *gnom$^{R5}$* seedlings were germinated and transferred to plates containing low concentrations of NAA (0.01-0.1 μM). Although root growth rates were slightly

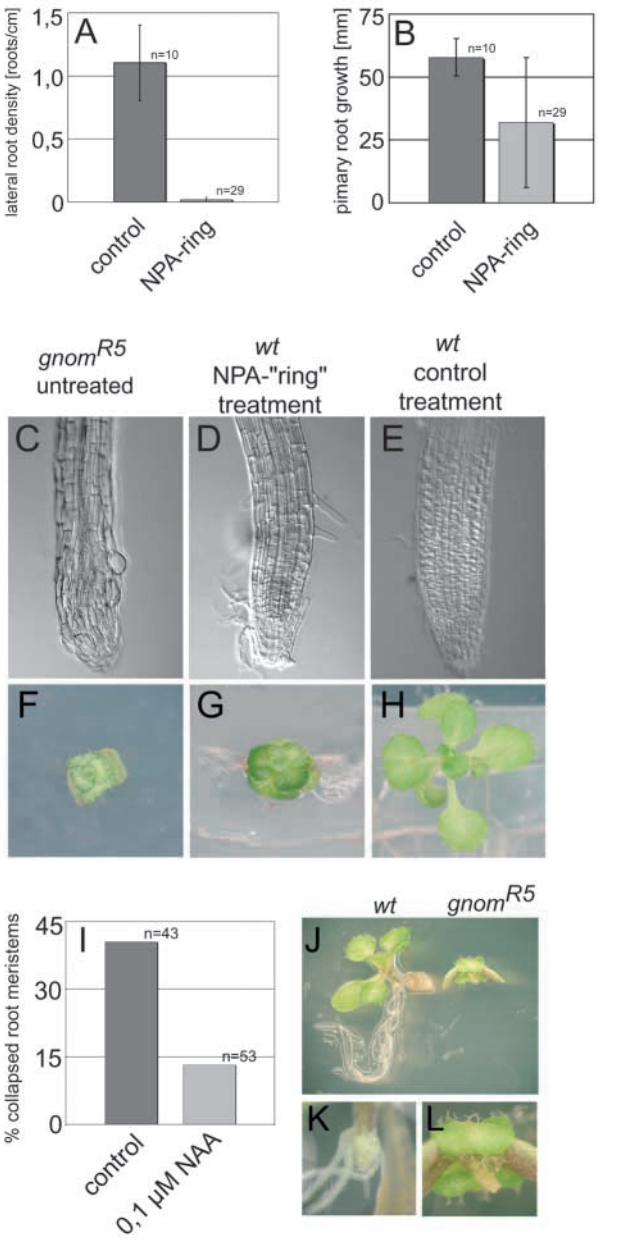


**Fig. 5.** Root growth phenotypes of *gnom$^{R5}$* roots are auxin-mediated. (A,B) Local application of NPA at the hypocotyl-root junction of wild-type roots severely reduces lateral root formation (A) and decreases primary root elongation (B). Plants were grown for 15 days. Differences between treatments were significant ($P$<0.001). (C-H) Comparison of (C-E) root tips and (F-H) rosette leaves after local application of NPA. (C,F) Untreated *gnom$^{R5}$*, (D,G) NPA-treated wild type, (E,H) DMSO-treated wild type (control). (I) *gnom$^{R5}$* root meristem collapse can be reduced by transferring seedlings to plates supplemented with NAA. Observed numbers were significantly different from each other ($P$<0.01). (J-L) Root regeneration of seedlings. (J) Comparison of wild-type (left) and *gnom$^{R5}$* (right), 9 days after cutting. (K,L) Magnification of regeneration zone of (K) wild type and (L) *gnom$^{R5}$*.

increased in *gnom$^{R5}$*, but slightly decreased in wild type (data not shown), a much more impressive improvement of primary root meristems was observed after 18 days of growth. Whereas

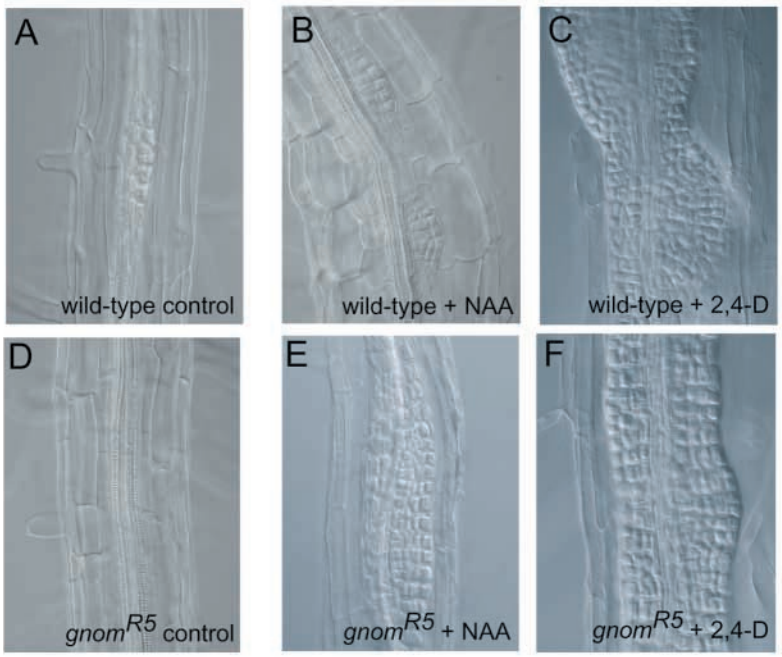


**Fig. 6.** Auxin induces disorganised pericycle divisions in *gnom$^{R5}$*. Lateral root primordia of (A-C) wild type and (D-F) *gnom$^{R5}$*, after 48 hours of treatment. (A,D) Control, (B,E) 0.1 μM NAA, (C,F) 0.1 μM 2,4-D.

approximately half of the *gnom$^{R5}$* roots on control plates were completely collapsed and nearly all had only very few meristematic cells left, less than 15% of NAA-treated root meristems were collapsed (Fig. 5I) and most of them were comparable to those of young *gnom$^{R5}$* plantlets (data not shown).

### *gnom$^{R5}$* seedlings cannot regenerate roots

*Arabidopsis* seedlings easily regenerate a root from the hypocotyl stump after surgical removal of the primary root. This adventitious root formation depends on polar auxin transport (Thimann, 1972). Transected seedlings grown on plates spontaneously regenerated a root within 3 days (data not shown), resulting in a complete root system after 9 days (Fig. 5J,K). Root regeneration was abolished by treatment with NPA (data not shown). *gnom$^{R5}$* seedlings were completely unable to regenerate a root after surgical removal of the primary root (Fig. 5J,L). None out of 20 seedlings showed any sign of root regeneration, even after 20 days of growth on plates. This result suggests a more stringent requirement of *GNOM* activity for post-embryonic root regeneration than for root meristem establishment during embryogenesis because all *gnom$^{R5}$* seedlings form a primary root during embryogenesis.

### GNOM is required for induction and organisation of lateral root primordia

The inability of *gnom$^{R5}$* seedlings to form lateral roots might result from insufficient auxin transport from apical tissues. Alternatively, *gnom$^{R5}$* might not respond correctly to auxin. To distinguish between these possibilities, we treated *gnom$^{R5}$* and wild-type roots with different auxin analogues for 24-48 hours and investigated their response in regard to lateral root induction. Untreated wild-type roots initiated widely spacing primordia (Fig. 6A). Treatment with 0.1 μM of the transportable auxin NAA (Delbarre et al., 1996) reduced the distance between individual root primordia, increasing their number (Fig. 6B), but did not affect their organisation. By contrast, the same concentration of the non-transportable auxin analogue 2,4-D caused proliferation of pericycle cells along large regions of the primary root. Individual root primordia were not distinct any more, and zones of more or less proliferation alternated, resulting in a 'wavy' appearance of the proliferation zone (Fig. 6C). Thus, transportable NAA and non-transportable 2,4-D had very different effects on lateral root induction. Untreated *gnom$^{R5}$* roots were completely devoid of lateral root primordia and lacked any sign of pericycle division (Fig. 6D). By contrast, exogenously supplied NAA induced homogenous proliferation of the pericycle layer in large regions of the root, and there was no indication of organised primordia growth, resembling wild-type roots treated with 2,4-D (Fig. 6E). 2,4-D treatment had very much the same effect on *gnom$^{R5}$* roots as NAA treatment, except that the induction of proliferation was even stronger. Thus, non-dividing pericycle cells of *gnom$^{R5}$* seedlings can be induced to divide when supplied with auxin, which strongly suggests that the failure to form lateral root primordia is due to a shortage of auxin in the primary root. In addition, it demonstrates that GNOM function is required for two steps of lateral root formation. First, there is a non-autonomous requirement of GNOM, in transporting auxin from above-ground tissues into the root in order to initiate lateral root primordia. Second, there is an autonomous requirement of GNOM in the pericycle layer itself to organise primordium outgrowth while laterally inhibiting proliferation of adjacent pericycle cells. The fact that *gnom$^{R5}$* roots responded to transportable auxin in much the same way as the wild-type did to a non-transportable auxin suggested that the *gnom$^{R5}$* phenotype may be the result of an inability to properly transport auxin required for the organised development of lateral root primordia. To correlate the observed disorganisation of incipient primordia with defects in polar auxin transport and establishment of auxin-response gradients, we analysed PIN1 localisation and *DR5::GUS* activity during lateral root formation. PIN1 expression was detected from the very beginning of lateral root development. In a stage I primordium, PIN1 was localised in a strictly polar fashion along the main root axis (Fig. 7A). Whether individual cells had their apical or basal end labelled could not be distinguished. Upon initiation of periclinal divisions, PIN1 maintained its polar localisation but was also seen at newly formed cell boundaries (Fig. 7B). As the root primordium became multi-layered, its inner cells showed a seemingly apolar distribution of PIN1 whereas peripheral cells displayed preferential labelling of PIN1 at the cell boundaries towards the tip of the incipient root primordium (Fig. 7C). This new polarity, orthogonal to the old axis of polarity, became more and more pronounced until PIN1 polar localisation was completely re-orientated towards the new tip of the emerging lateral root primordium (Fig. 7D). *DR5::GUS* signals were also

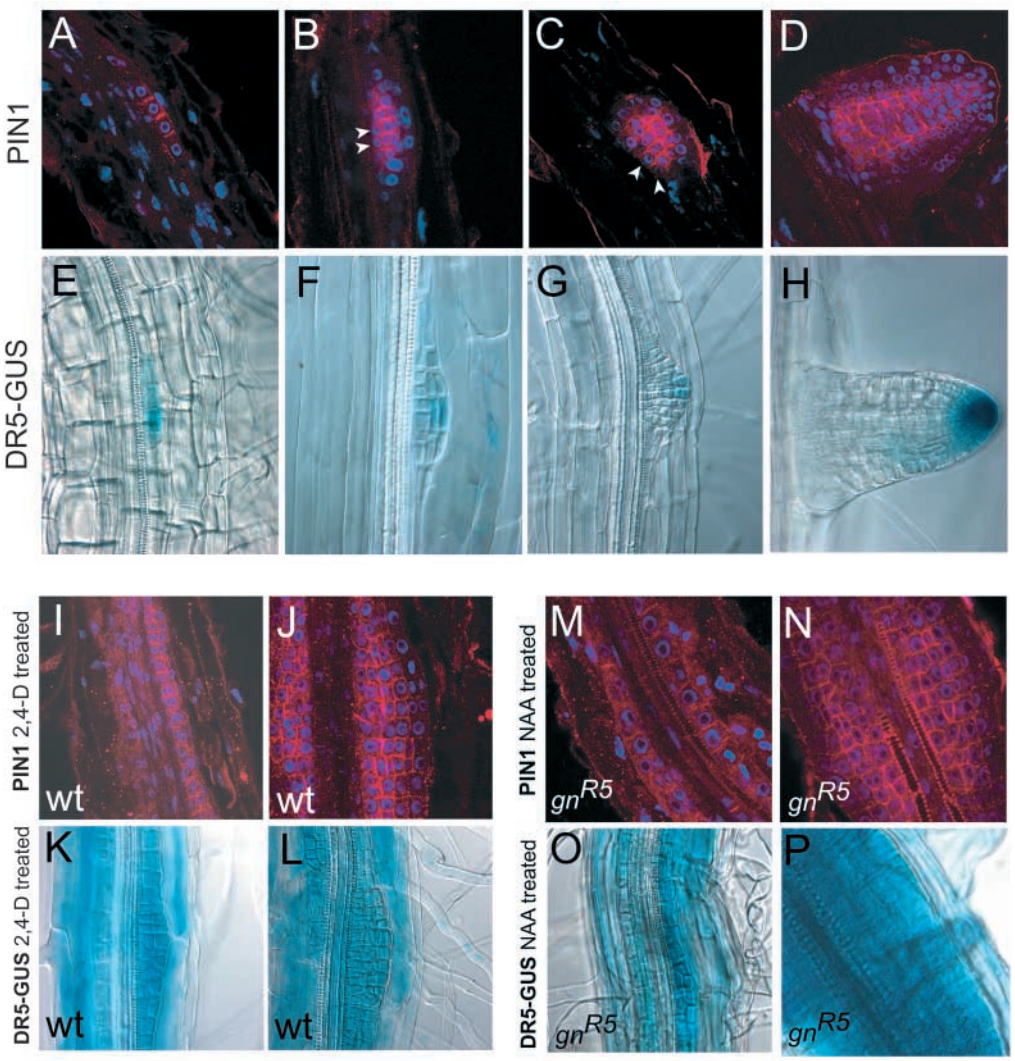


**Fig. 7.** *gnom*$^{R5}$ defects in lateral root formation correlate with an inability to establish transport-dependent auxin-response gradients. (A-H) Different stages of wild-type lateral root development. (A-D) PIN1 signals, (E-H) *DR5::GUS* signals. (A,E) stage I, (B,F) stages III-IV, (C,G) stage VI, (D,H) emerged lateral root. Arrows indicate borders of peripheral cells without PIN1. Staging according to Malamy and Benfey (Malamy and Benfey, 1997). (I-L) Wild-type treated with 0.1 μM 2,4-D. (I,J) PIN1 signals, (K,L) *DR5::GUS* signals. (I,K) One- or two-layered dividing pericycle, (J,L) multi-layered division zone. (M-P) *gnom*$^{R5}$ treated with 0.1 μM NAA. (M,N) PIN1 signals, (O,P) *DR5::GUS* signals. (M,O) One- or two-layered dividing pericycle, (N,P) multi-layered division zone.

observed in stage I primordia, with the strongest staining often located in the centre of the young primordium (Fig. 7E). Upon periclinal divisions, this central staining was shifted to a more distal region of the primordium (Fig. 7F,G). In the emerging lateral root *DR5::GUS* activity was strongest distally, which resembled the situation in the primary root tip (Fig. 7H) (Sabatini et al., 1999). Thus, the presumed direction of auxin flow, as inferred from PIN1 polar localisation, was consistent with the establishment of an adjacent maximum auxin response. A more detailed description of the relationship between expression and localisation of several PIN proteins and auxin gradient establishment is given elsewhere (Benková et al., 2003). NAA treatment did not alter PIN1 localisation or *DR5-GUS* distribution, except that the *DR5::GUS* signal was increased (data not shown). By contrast, 2,4-D treatment induced PIN1 expression in long stretches of dividing pericycle cells. Although PIN1 localisation was initially similar to untreated controls (Fig. 7I), it subsequently became more and more randomised and the gradual re-orientation of polarity did not occur (Fig. 7J). In parallel, young and older 'primordia' of 2,4-D-treated roots had homogenous *DR5::GUS* staining (Fig. 7K,L). Similar abnormalities of PIN1 localisation and *DR5::GUS* staining were also observed in NAA-treated *gnom*$^{R5}$ roots. PIN1 localisation, although initially polar (Fig. 7M), became more and more depolarised and no re-orientation of polarity was detected (Fig. 7N). In addition, no gradients of *DR5::GUS* activity were established at any stage in the developing multi-layered proliferation zone (Fig. 7O,P). Thus, *gnom*$^{R5}$ is defective in organising polar auxin transport required for proper initiation and development of lateral root primordia.

## Discussion

Mutant analysis of genes involved in fundamental patterning processes is often limited by an early developmental arrest, which precludes the study of gene function during subsequent development. In addition, it is difficult to distinguish between primary and secondary consequences of loss of gene function when the body organisation of the mutant is already severely perturbed during early development. Both of these considerations apply to *GNOM* as strong mutant alleles interfere with embryo patterning, resulting in grossly abnormal seedlings (Mayer et al., 1993). We have now shown that *GNOM* is continually expressed in proliferating and developing tissues during post-embryonic development,

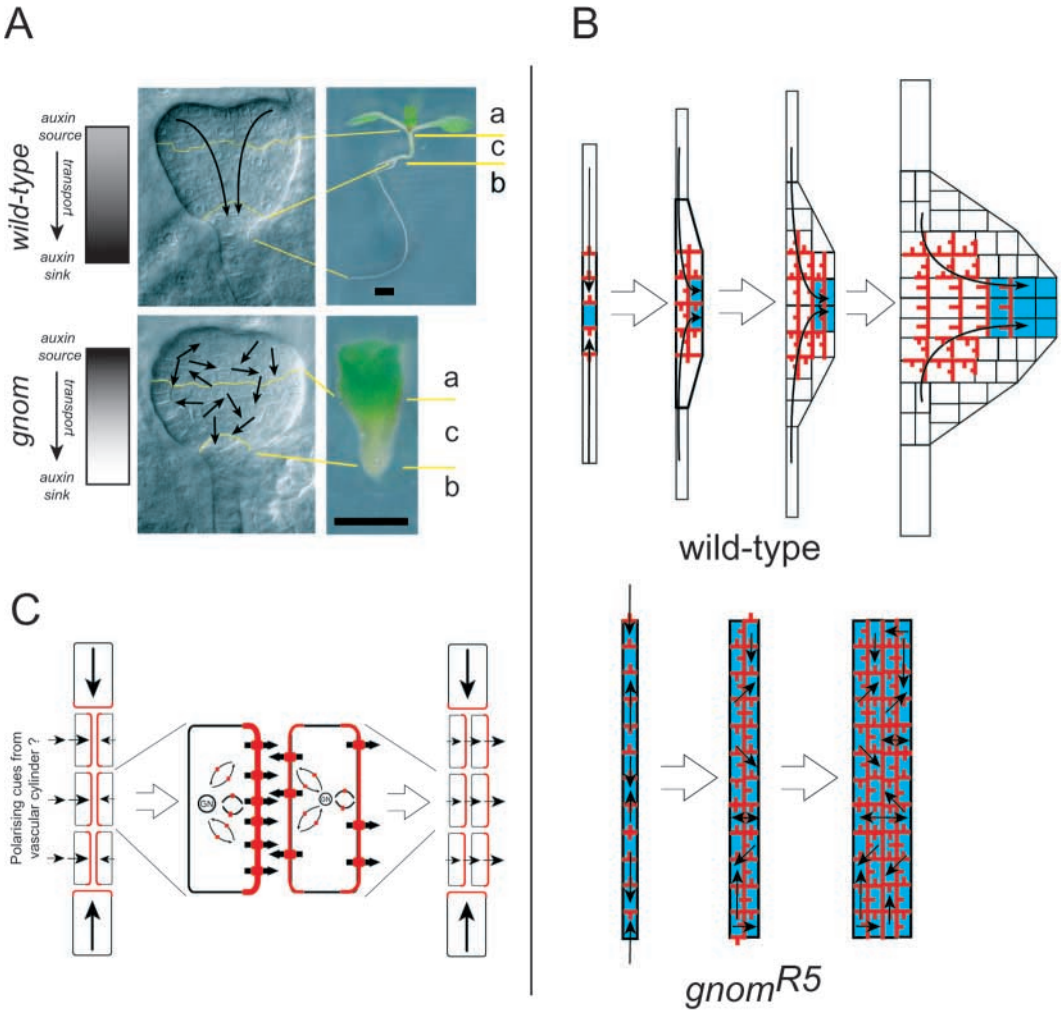


**Fig. 8.** A speculative model for GNOM action – canalising auxin fluxes. (A) Heart-stage embryos of wild-type (top) and strong *gnom* allele (bottom). Yellow lines delineate the apical (a), central (c) and basal (b) regions of the embryos and their relation to the body pattern of the seedling (right). Black arrows indicate auxin flow from sources in the apical part of the embryo to the sink in the basal part. Presumed auxin gradients are shown at the left. (B) Relationship between localisation of PIN1 efflux carrier (red) and auxin-response gradients (blue) in lateral root primordium development. Arrows indicate auxin canalisation by gradual re-orientation of individual transport polarities of cells. Red stubs touching a given cell boundary mark the cell to which the respective PIN1 label is thought to belong. (C) Presumptive critical step for the canalisation of auxin flow during lateral root formation. Stage II lateral root primordium immediately after division is shown at the left, with the two daughter cell layers displaying opposite polarities. Gradual, GNOM-dependent, relocalisation of efflux carriers might be guided by weak polarising cues from adjacent tissues, supplying more auxin to the inner layer, which then imposes its auxin transport polarity on the outer layer. Arrows indicate direction of auxin flux; auxin efflux carriers (PIN1; in red); GN, GNOM-positive endosomes involved in recycling auxin carriers.

suggesting a role for GNOM during the entire life cycle of *Arabidopsis*. Consistent with this, a GNOM variant that is resistant to the action of brefeldin A (BFA), a vesicle transport inhibitor, confers insensitivity to BFA-induced inhibition of cellular and developmental processes, such as PIN1 cycling, primary root elongation, lateral root induction, gravitropism and polar auxin transport in inflorescences (Geldner et al., 2003). However, these experiments could not determine whether GNOM plays a necessary role in post-embryonic development and what phenotypes would result from a compromised *GNOM* function.

## Nearly all developmental phenotypes in weak *gnom* lines can be explained by defects in auxin transport

Our phenotypic analysis of the $gnom^{R5}$ allele and the weaker $gnom^{B/E}$ allelic combination revealed an impressive number of auxin-related phenotypes that correlated with residual *GNOM* function. Disorganised vascular tissue, fusion of cotyledons, leaf epinasty, inhibition of leaf blade expansion, dwarfed stature, short roots and inhibition of lateral root formation were all observed, not only in $gnom^{R5}$, but also, to a lesser extent, in the weaker $gnom^{B/E}$ line. Some of these phenotypes as well as the observed defect in root gravitropism are clearly auxin transport-mediated responses, whereas others, such as variably delayed flowering and delayed senescence cannot be, to our knowledge, immediately attributed to reduced auxin transport. The stunted primary inflorescence combined with an increased number of secondary inflorescences superficially resembles reduced apical dominance as observed in auxin transport mutants (Noh et al., 2001; Ruegger et al., 1997). The altered dynamics of lateral inflorescence formation, however, might also be a secondary consequence of delayed senescence or an earlier growth arrest of the primary inflorescence rather than a direct effect of reduced auxin transport.

The observed collapse of the primary root meristem in $gnom^{R5}$ can be explained by an insufficient supply of auxin to the root tip, which would lead to cell-cycle arrest due to auxin depletion and subsequent differentiation. We confirmed this notion by phenocopying the mutant phenotype through NPA treatment of wild-type roots at the hypocotyl-root junction and by partially rescuing the $gnom^{R5}$ phenotype through auxin application. Furthermore, we demonstrated a reduced capacity

of *gnom*$^{R5}$ root tips to maintain auxin-response gradients when challenged with auxin. Thus, reduction of *GNOM* function impairs polar auxin transport in post-embryonic development.

### A model of GNOM action that explains the diverse developmental phenotypes of the mutant

We would like to propose a common model of GNOM action to account for three major aspects of the *gnom* phenotype: (1) disorganisation of the vascular tissue, which is gradually relieved in plants with the weaker alleles, (2) embryonic axis formation defects, which are exclusively observed in those with strong alleles, and (3) inability to form organised root primordia in response to auxin, which is apparent in *gnom*$^{R5}$.

We assume that GNOM is a central player in a positive feedback loop between auxin distribution and transport polarity. Such a feedback loop was postulated in the canalisation hypothesis, initially proposed to explain vascular tissue patterning in plants (Sachs, 1988; Sachs, 1991). It essentially states that auxin can lead to the gradual establishment of auxin channels in a field of initially homogeneous cells, resulting in the eventual differentiation of vascular tissues. In this theory, auxin itself is a limiting factor that induces auxin transport capacity and polarity. Initially random transport polarities would be orientated and amplified by inducing adjacent cells to polarise in the same direction, which would improve transport efficiency along a given vector. Establishment of an efficient auxin channel would not only increase the probability of inducing the same polarity downstream but also deplete auxin from surrounding cells, decreasing their chances to become channels themselves. The Sachs theory has been discussed in great detail, and it has been pointed out that this theory can in priniciple be extended to a large number of organogenic processes in plants (Berleth et al., 2000; Berleth and Sachs, 2001).

In cell-biological terms, this canalisation hypothesis necessitates that a plant cell is able to sense an unequal distribution of auxin and to translate it into an accumulation of efflux carriers at the end away from the external auxin maximum. For efficient polarisation in response to external cues, the cell needs to continuously re-direct vesicular trafficking of carriers to specific regions of the plasma membrane. Mutations in *GNOM* interfere either with the activities of the carriers per se or their polar localisation (or both at the same time) and could thus disrupt the positive feedback loop needed for the organisation of tissues and organs.

The vascular patterning defects of *gnom* are consistent with such a role. This was noted before by Koizumi et al. (Koizumi et al., 2000), who identified a new *gnom* allele in a screen for vascular pattern mutants, and will therefore not be discussed here. In the following, we want to describe how a similar mechanism can also account for the *gnom* defects in embryo axis establishment and lateral root formation.

Strong *gnom* alleles produce three major embryonic phenotypes: fusion of cotyledons, general thickening of cotyledons and hypocotyl, and deletion of the root. These phenotypes are simultaneously restored in plants with weak *gnom* alleles, suggesting a common primary defect that we propose is a grossly perturbed alignment of individual auxin-transport polarities (Fig. 8A). As a consequence, the basal part of the embryo would lack the auxin needed to induce a root meristem. In addition, auxin would accumulate in the presumptive sites of synthesis in the apical part, leading to cotyledon fusion. Also, an insufficient auxin flow through the central part would lead to randomised cell division and expansion, causing thickening of the axis.

Embryogenesis is essentially normal in weak *gnom* mutants. Although a primary root is always formed in *gnom*$^{R5}$, no organised lateral root primordia are established. Formation of a lateral root primordium necessitates re-establishment of cell division and elongation patterns orthogonal to the old root axis, as illustrated by the gradual repolarisation of PIN1 (Fig. 8B), which does not occur in *gnom*$^{R5}$. We propose that this process also utilises a canalisation-like mechanism: polar auxin transport accumulates auxin in some cells of the pericycle layer which then proliferate and deplete auxin from adjacent cells, inhibiting their proliferation (Fig. 8B). For this, we assume that PIN1 localisation in a stage I primordium is organised in a bipolar fashion (Fig. 8B), which, in our view, is the only way to explain the simultaneous peak of auxin response within the primordium and auxin-mediated lateral inhibition. Failure to do so would lead to homogeneous proliferation of the pericycle upon auxin addition, as observed in *gnom*$^{R5}$. In addition, *gnom*$^{R5}$ is unable to re-orientate PIN1 polarity orthogonal to the old axis. The periclinal orientation of cell divisions in stage I primordia would inherently shift polarity since PIN1 localises to newly forming cell plates (Geldner et al., 2001). However, this would lead to an unstable situation immediately after division, with the daughter cells displaying opposite PIN1 polarities (Fig. 8C). We propose that a weak bias in auxin supply switches the polarity of one of the daughter cells and that GNOM is critical at this step. Once two equally polarised cells are established, new breaks in polarity during subsequent periclinal divisions would be restored to the direction set by the two precursor cells. This would eventually lead to the 90° shift in polarity observed in wild-type. Flattening of auxin gradients by 2,4-D treatment would have the same effect as reduced *GNOM* function, both disrupting an auxin-canalising feedback loop, which results in disorganised efflux carrier localisation and randomised proliferation.

The model outlined above provides a coherent framework for the diverse roles of GNOM action in development. In the future, the partial loss-of-function *gnom* alleles may also prove useful to genetically dissect the diverse developmental roles of auxin transport and to explore the applicability of the canalisation hypothesis in organ patterning.

We wish to thank Tom Guilfoyle and Klaus Palme for providing the *DR5::GUS* reporter line and PIN1 antiserum, respectively. We thank Wolfgang Kornberger for technical assistance, Wolfgang Haupt for initial characterisation of *gnom*$^{R5}$ and Nadine Anders, Jiří Friml, Dolf Weijers and Hanno Wolters for comments on the manuscript. We are grateful to Eva Benkova for discussion and sharing of unpublished data. This work was supported by the Deutsche Forschungsgemeinschaft (SFB 446, A9).

## References

**Benková, E., Michniewicz, M., Sauer, M., Teichmann, T., Seifertová, D., Jürgens, G. and Friml, J.** (2003). Local, efflux-dependent auxin gradients as a common module for plant organ formation. *Cell* **115**, 591-602.

**Berleth, T. and Jürgens, G.** (1993). The role of the monopteros gene in organising the basal body region of the *Arabidopsis* embryo. *Development* **118**, 575-587.

**Berleth, T., Mattsson, J. and Hardtke, C. S.** (2000). Vascular continuity and auxin signals. *Trends Plant Sci.* **5**, 387-393.

**Berleth, T. and Sachs, T.** (2001). Plant morphogenesis: long-distance coordination and local patterning. *Curr. Opin. Plant Biol* **4**, 57-62.

**Busch, M., Mayer, U. and Jürgens, G.** (1996). Molecular analysis of the Arabidopsis pattern formation gene GNOM: Gene structure and intragenic complementation. *Mol. Gen. Genet.* **250**, 681-691.

**Casimiro, I., Beeckman, T., Graham, N., Bhalerao, R., Zhang, H., Casero, P., Sandberg, G. and Bennett, M. J.** (2003). Dissecting Arabidopsis lateral root development. *Trends Plant Sci.* **8**, 165-171.

**Delbarre, A., Muller, P., Imhoff, V. and Guern, J.** (1996). Comparison of mechanisms controlling uptake and accumulation of 2,4-dichlorophenoxy acetic acid, naphthalene-1-acetic acid, and indole-3-acetic acid in suspension-cultured tobacco cells. *Planta* **198**, 532-541.

**Donaldson, J. G. and Jackson, C. L.** (2000). Regulators and effectors of the ARF GTPases. *Curr. Opin. Cell Biol.* **12**, 475-482.

**Friml, J., Benkova, E., Blilou, I., Wisniewska, J., Hamann, T., Ljung, K., Woody, S., Sandberg, G., Scheres, B., Jürgens, G. and Palme, K.** (2002). AtPIN4 mediates sink-driven auxin gradients and root patterning in Arabidopsis. *Cell* **108**, 661-673.

**Gälweiler, L., Guan, C., Müller, A., Wisman, E., Mendgen, K., Yephremov, A. and Palme, K.** (1998). Regulation of polar auxin transport by AtPIN1 in Arabidopsis vascular tissue. *Science* **282**, 2226-2230.

**Geldner, N., Anders, N., Wolters, H., Keicher, J., Kornberger, W., Muller, P., Delbarre, A., Ueda, T., Nakano, A. and Jürgens, G.** (2003). The Arabidopsis GNOM ARF-GEF mediates endosomal recycling, auxin transport, and auxin-dependent plant growth. *Cell* **112**, 219-230.

**Geldner, N., Friml, J., Stierhof, Y. D., Jürgens, G. and Palme, K.** (2001). Auxin transport inhibitors block PIN1 cycling and vesicle trafficking. *Nature* **413**, 425-428.

**Geldner, N., Hamann, T. and Jürgens, G.** (2000). Is there a role for auxin in early embryogenesis? *Plant Growth Regulation* **32**, 187-191.

**Grebe, M., Gadea, J., Steinmann, T., Kientz, M., Rahfeld, J. U., Salchert, K., Koncz, C. and Jürgens, G.** (2000). A conserved domain of the Arabidopsis GNOM protein mediates subunit interaction and cyclophilin 5 binding. *Plant Cell* **12**, 343-356.

**Hadfi, K., Speth, V. and Neuhaus, G.** (1998). Axin-induced developmental patterns in Brassica juncea embryos. *Development* **125**, 879-887.

**Jürgens, G.** (2001). Apical-basal pattern formation in Arabidopsis embryogenesis. *EMBO J.* **20**, 3609-3616.

**Koizumi, K., Sugiyama, M. and Fukuda, H.** (2000). A series of novel mutants of *Arabidopsis thaliana* that are defective in the formation of continuous vascular network: calling the auxin signal flow canalization hypothesis into question. *Development* **127**, 3197-3204.

**Lauber, M. H., Waizenegger, I., Steinmann, T., Schwarz, H., Mayer, U., Hwang, I., Lukowitz, W. and Jürgens, G.** (1997). The Arabidopsis KNOLLE protein is a cytokinesis-specific syntaxin. *J. Cell Biol.* **139**, 1485-1493.

**Liu, C. M., Xu, Z. H. and Chua, N. H.** (1993). Auxin polar transport is essential for the establishment of bilateral symmetry during early plant embryogenesis. *Plant Cell* **5**, 621-630.

**Malamy, J. E. and Benfey, P. N.** (1997). Organization and cell differentiation in lateral roots of *Arabidopsis thaliana*. *Development* **124**, 33-44.

**Mayer, U., Büttner, G. and Jürgens, G.** (1993). Apical-basal pattern formation in the *Arabidopsis* embryo: Studies on the role of the *gnom* gene. *Development* **117**, 149-162.

**Muller, H. J.** (1932). *Further Studies on the Nature and Causes of Gene Mutations.* Proceedings of the 6th International Congress of Genetics **1**, 213-255.

**Noh, B., Murphy, A. S. and Spalding, E. P.** (2001). Multidrug resistance-like genes of Arabidopsis required for auxin transport and auxin-mediated development. *Plant Cell* **13**, 2441-2454.

**Nüsslein-Volhard, C., Lohs-Schardin, M., Sander, K. and Cremer, C.** (1980). A dorso-ventral shift of embryonic primordia in a new maternal-effect mutant of Drosophila. *Nature* **283**, 474-476.

**Reed, R. C., Brady, S. R. and Muday, G. K.** (1998). Inhibition of auxin movement from the shoot into the root inhibits lateral root development in Arabidopsis. *Plant Physiol.* **118**, 1369-1378.

**Roth, S., Stein, D. and Nüsslein-Volhard, C.** (1989). A gradient of nuclear localization of the dorsal protein determines dorsoventral pattern in the Drosophila embryo. *Cell* **59**, 1189-1202.

**Rubery, P. H. and Sheldrake, A. R.** (1974). Carrier-mediated auxin transport. *Planta* **118**, 101-121.

**Ruegger, M., Dewey, E., Hobbie, L., Brown, D., Bernasconi, P., Turner, J., Muday, G. and Estelle, M.** (1997). Reduced naphthylphthalamic acid binding in the tir3 mutant of Arabidopsis is associated with a reduction in polar auxin transport and diverse morphological defects. *Plant Cell* **9**, 745-757.

**Sabatini, S., Beis, D., Wolkenfelt, H., Murfett, J., Guilfoyle, T., Malamy, J., Benfey, P., Leyser, O., Bechtold, N., Weisbeek, P. and Scheres, B.** (1999). An auxin-dependent distal organizer of pattern and polarity in the Arabidopsis root. *Cell* **99**, 463-472.

**Sachs, T.** (1988). Epigenetic selection: an alternative mechanism of pattern formation. *J. Theor. Biol.* **134**, 547-559.

**Sachs, T.** (1991). Cell polarity and tissue patterning in plants. *Development* **Supplement 1**, 83-93.

**Shevell, D. E., Leu, W. M., Gillmor, C. S., Xia, G., Feldmann, K. A. and Chua, N. H.** (1994). EMB30 is essential for normal cell division, cell expansion, and cell adhesion in Arabidopsis and encodes a protein that has similarity to Sec7. *Cell* **77**, 1051-1062.

**Shevell, D. E., Kunkel, T. and Chua, N. H.** (2000). Cell wall alterations in the Arabidopsis *emb30* mutant. *Plant Cell* **12**, 2047-2060.

**Skoog, F. and Miller, C. O.** (1957). Chemical regulation of growth and organ formation in plant tissue culture in vitro. *Symp. Soc. Exp. Biol.* **11**, 118-131.

**Steinmann, T., Geldner, N., Grebe, M., Mangold, S., Jackson, C. L., Paris, S., Gälweiler, L., Palme, K. and Jürgens, G.** (1999). Coordinated polar localization of auxin efflux carrier PIN1 by GNOM ARF GEF. *Science* **286**, 316-318.

**Taiz, L. and Zeiger, E.** (1998). *Plant Physiology*, 2nd ed. Sunderland: Sinauer Associates Inc.

**Thimann, K. V.** (1972). The natural plant hormones. In *Plant Physiology: A Treatise* (ed. F. C. Steward), Volume VI, Chapter 5. New York: Academic Press.

**Ulmasov, T., Murfett, J., Hagen, G. and Guilfoyle, T. J.** (1997). Aux/IAA proteins repress expression of reporter genes containing natural and highly active synthetic auxin response elements. *Plant Cell* **9**, 1963-1971.

**Went, F. W.** (1929). Wuchsstoff und Wachstum. *Recueil des travaux botaniques neerlandais* **XXV**, 1-117.